The Sun as an X–ray Star IV: The Contribution of Different Regions of the Corona to its X–ray Spectrum

S. Orlando
Osservatorio Astronomico di Palermo "G.S. Vaiana",
Piazza del Parlamento 1, I–90134 Palermo, Italy

G. Peres, and F. Reale
Dip. di Scienze Fisiche ed Astronomiche – Sez. di Astronomia –
Univ. di Palermo, Piazza del Parlamento 1, I–90134 Palermo, Italy

ABSTRACT

We study X–ray synthesized spectra of solar regions as templates to interpret analogous stellar spectra. We define three classes of coronal structures of different brightness, low (background quiet corona), medium (active regions), high (active regions cores), and determine their contribution to the solar X–ray emission measure vs. temperature, EM(T), luminosity and spectrum. This study defines the extent of the solar analogy quantitatively and accurately.

To this end, we have selected a large sample of full–disk Yohkoh/SXT observations taken between the maximum and the minimum of solar cycle 22, obtaining the contribution of each class to the whole Sun's EM(T). From the EM(T) distributions we synthesize the X–ray spectra of the Sun and of the single classes of solar coronal regions as they would be collected with ROSAT/PSPC and ASCA/SIS. We find that the Sun during the cycle fits well in the stellar scenario as a low activity star. The ROSAT/PSPC hardness ratio HR and surface X–ray flux F_{PSPC} both increase going from the background corona to the active regions, to the cores of active regions, and range between the values of low and intermediate activity stars. We suggest that the coronae of these stars may be explained as the effect of structures similar to those present on the Sun and that the various levels of X–ray luminosity, HR and F_{PSPC} are achieved changing the surface coverage of the different classes of coronal regions.

Subject headings: Sun: activity, Sun: corona, stars: activity, stars: coronae

1. Introduction

The Sun is the only late–type star we can study in great detail and, for this reason, it can be used as a template to interpret X–ray observations of late–type stars, assuming that the physical processes governing the coronae of these stars are similar to those leading the solar corona (the so–called "solar–stellar connection"). Given the impact of this assumption on stellar physics, it is therefore natural to ask: how far does the solar model apply to other stars? how do the underlying processes differ? or, in other words, how realistic is this assumption?

Answering the questions raised above is important because comparing solar and stellar results may be fundamental to understand the physical mechanisms governing the solar corona and the coronae of late–type stars. Solar and stellar observations provide us with complementary information: the former yields a very detailed physical scenario of the phenomena occurring in corona, the latter a larger variety of phenomena and physical conditions. The stellar observations replace the advantages of spatial resolution with the ability to range physical parameters which the Sun does not allow us to change as, for example, the rotation rate or the photospheric temperature; thanks to stars we can explore the parameter space necessary to uncover fundamental features of coronal activity. A classical example is the well established relationship between the rotation rate of the star and its activity (Pallavicini et al. 1981) discovered thanks to the analysis of a sample of stellar data.

In the light of the above considerations, we are pursuing a project to study the Sun as an X–ray star, and using the solar data as a guide and a template for stellar observations. To this end, we developed a method, described in Orlando et al. (2000a, hereafter Paper I) and in Peres et al. (2000a – Paper II), to put the solar data collected with the Soft X–ray Telescope (SXT) on board Yohkoh[1] (Tsuneta et al. 1991) into a format and context virtually identical to that of stellar X–ray observations as those collected, for instance, with ROSAT/PSPC (i.e. the Position Sensitive Proportional Counter on board the Roentgen Satellit) or ASCA/SIS (i.e. the Solid–state Imaging Spectrometer on board the Advanced Satellite for Cosmology and Astrophysics). In Paper II, we considered a few representative examples of solar observations at different moments of the solar cycle, applying the standard methods of analysis used for stellar observations to the synthesized stellar–like data and comparing the results with those of stellar X–ray studies.

In this paper, we expand the set of cases studied to a relatively large number and investigate the contribution of different coronal regions on the Sun to the emission measure distribution vs. temperature, EM(T), in different phases of the solar activity, and to the corresponding stellar–like synthesized X–ray spectra. Since the solar corona is spatially resolved, we are able to identify the sources of X–ray emission in the solar corona, with the potential to identify the coronal regions responsible for some features observed on stars, and to link some phenomena (or structures) we observe on the Sun with features in the stellar data. We exclude solar flares from our analysis, their detailed analysis being the subject of another paper (Reale et al. 2000).

Our main aim is to define quantitatively and accurately the extent of the solar analogy, using real data and making very few model assumptions. This study will allow us to put the physics of

---

[1]Yohkoh was launched at the end of 1991 during the maximum of the solar activity and it is still in operation. Through almost one decade of observations, it has given us a wealth of X–ray images, in particular a unique sequence of daily X–ray images of the Sun, covering a complete solar cycle and observing a large variety of phenomena.

the solar corona in the context of stellar coronal physics and to explore whether the large range of activity levels and X–ray luminosity observed in late–type stars can be explained in terms of different relative weights of various coronal structures present on the stars, e.g. quiet background regions, active regions, and active regions cores. Along this line, Drake et al. (2000) compared the EM(T) derived for different classes of coronal regions on the solar disk, with the observed stellar EM(T) distributions of two intermediate activity stars. They found that the peak temperature and the slope of the stellar EM(T) distributions are very similar to those of active regions cores, supporting the hypothesis that the high level of activity of these stars is due to active regions being the dominant structures on the star. Drake et al. (2000) based their study on one sequence of observations collected by Yohkoh/SXT at a single moment, the maximum of the solar cycle. In this paper we consider a wider sample of solar data, studying well identified coronal regions as well as their contribution to the global coronal emission, during the whole solar cycle. We will show that the comparison of our results with the stellar findings in literature gives us some interesting hints to explain the large range of activity level characterizing the late–type stars as different combinations of solar–like regions, similarly to Drake et al. (2000).

In Sect. 2 of this paper, we summarize our method to study the Sun as an X–ray star; in Sect. 3 we present the sample of Yohkoh/SXT data selected for our analysis, and describe our criterion to isolate different regions on the solar corona; in Sect. 4 we investigate the contributions of the different regions to the whole corona EM(T) distributions and their evolution along the solar cycle; the synthesis of ROSAT/PSPC and ASCA/SIS spectra from the EM(T) distributions is discussed in Sect. 5 together with their analysis, and the correlation between the X–ray surface fluxes and the spectral hardness ratio for the ROSAT/PSPC spectra; finally in Sect. 6 we discuss our findings and draw our conclusions.

2. The Method

In this section we summarize the main steps of our method. We refer the reader to the Papers I and II for more details.

Our approach is based on solar observations made with Yohkoh/SXT. The standard analysis of Yohkoh/SXT images taken through two different filters allows to derive the temperature T and the emission measure EM in every pixel of the images of the corona[2]. From the relevant spatially resolved maps of temperature T and emission measure EM, we derive the distribution

[2]In Paper I and II we have explored the relevant limitations in deriving the maps of temperature and emission measure using the filter ratio method: we derive the line–of–sight average isothermal temperature and emission measure in each pixel, assuming no variations of T within the field of view of a single pixel; we assume that the plasma is steady and under ionization equilibrium. For our task of comparing the X–ray solar spectrum with the low resolution spectra of other stars, we do not expect that the above assumptions have a large effect on the average EM(T).

of emission measure vs. temperature, EM(T): we divide the nominal range of temperature ($5.5 \leq \log T(\mathrm{K}) \leq 8$) to which SXT is sensitive into 29 bins, all equal on a logarithmic scale and appropriate to the spectral discriminating power of SXT; the emission measure of all the pixels belonging to the same temperature bin is then summed. We reject all the pixels with the photon count $n_{\mathrm{phot}} \leq 10$ to maintain an appropriate signal to noise ratio. The EM(T) distribution is important by itself for solar studies: for instance, it shows the contribution of the coronal plasma at different temperatures in determining the X–ray emission (cf. Paper II; Watanabe et al., 1995).

As a second step, we "put the Sun at stellar distances" and synthesize stellar–like spectra from the EM(T) distributions, using the MEKAL spectral synthesis code (Kaastra 1992; Mewe et al. 1995). The spectra are then folded through the instrumental response of the non–solar instruments of interest, obtaining the relevant stellar–like focal plane spectra. In the present work, we synthesize ROSAT/PSPC and ASCA/SIS observations which can be compared to a large sample of stellar coronal observations. The photon counts in each energy channel of the spectra synthesized are randomized according to Poisson statistics.

The synthesized spectra can be analyzed with the standard tools used for stellar X–ray observations and the relevant results can be compared directly with those obtained for real stars.

3. The Yohkoh/SXT Sample

We selected a sample of full–disk observations collected with SXT between December 1991 and April 1996, i.e. from the maximum to the minimum of solar cycle 22. In order to cover the dynamic range of the corona X–ray brightness, much larger than that of the CCD in the focal plane of SXT, each observing sequence includes images of different exposure times. Typically, standard observing sequences outside flares contain image in the thin aluminum (Al 1265 Å, referred to as Al.1) and the Al/Mg sandwich (comprising Al 2930 Å, Mg 2070 Å, Mn 562 Å, and C 190 Å, referred to as AlMg) filter bands. This set of filters allows us to derive maps of temperature (within $\sim 3 \times 10^5$ K – $\sim 10^7$ K) and emission measure for the whole corona (Tsuneta et al. 1991; Papers I and II).

Figure 1 shows the total coronal light curve in the Al.1 filter band obtained from the SXT Log database; the data we selected are marked with a cross. As evident from the figure, our sample of data is representative of different moments of the corona during the solar cycle. We applied the method outlined in Sect. 2 to all the data of our sample and we obtained the EM(T) distribution of the whole solar corona for each observing sequence.

3.1. Selection of the Coronal Structures

For our analysis, we identified three different classes of coronal regions contributing to the X–ray emission of the whole corona (hereafter WSC): the quiet regions (hereafter background corona, BKC), the active regions (ARs), and the active regions cores (COs). In order to select these regions in the Yohkoh/SXT images, we adopted a criterion based on the surface brightness I. We first derived the histogram of intensity values in the pixels of all the composite images in the filter band Al.1 of our sample; the intensity range has been divided into 50 bins of constant $\delta \log I \sim 0.1$ (Fig. 2). The histogram has a shape similar to that found by Hara (1996) with an ascent to a maximum value, followed by a power law descent (with a slope -0.75 ± 0.01) and, then, by a much steeper fall.

With the perspective to select regions on the Sun using their intrinsic properties, we chose the maximum at $I = 40$ DN s^{-1} and the significant change of shape at $I = 6 \times 10^3$ DN s^{-1} pixel^{-1} as discriminating values between different surface brightness values and, likely, intrinsic plasma conditions[3]. We have defined the lowest I regions the BKC, the intermediate I the ARs, and the highest I regions the COs. We have checked that this classification corresponds, indeed, to the common sense classification, as viewed directly on the images.

4. The EM(T) Distribution During the Solar Cycle

All the SXT data of our sample were first processed according to the standard Yohkoh analysis software: standard corrections (data decompression, dark current subtraction, pin–hole visible stray light subtraction), then image alignment, removal of the cosmic rays spikes, and vignetting correction. Then, we derived the EM(T) distributions of the WSC and of the coronal regions selected, applying the method outlined in Sect. 2.

Each sequence analyzed contains around twenty images. In most cases, this fact allowed us to derive from three to four EM(T) distributions of the corona per sequence and, therefore, to analyze the constancy of EM(T) *outside flares* on time scales of hours. We have found that, in all the cases analyzed, the EM(T) distributions appear practically steady on these time scales.

As anticipated in Paper II, the EM(T) distribution of the WSC is subject to large variations during the solar cycle. The shape of the EM(T) has always the same general trend, increasing monotonically until $T \sim 10^6$ K, reaching a maximum between 1 and 2 $\times 10^6$ K, and then decreasing monotonically towards higher temperatures. The main characteristics of the evolution of the EM(T) from maximum to minimum of solar activity are: a) the temperature of maximum emission

[3]Note that Hara (1996) instead chose a threshold at $I \sim 10^2$ DN s^{-1} pixel^{-1} between active regions from other darker regions. We have found that the results of our analysis do not change appreciably adopting a threshold $I \sim 40$ DN s^{-1} pixel^{-1} or $I \sim 10^2$ DN s^{-1} pixel^{-1}.

measure shifts from $T \sim 2 \times 10^6$ K to $T \sim 8 \times 10^5$ K; b) the EM(T) decreases by orders of magnitude; c) the slope of the descending part of the EM(T) gets steeper during the minimum of the cycle.

To help us to characterize the evolution of the EM(T) during the solar cycle we use an emission–measure–weighted temperature, as

$$< T >= \frac{\sum_i T_i \ \mathrm{EM}_i}{\sum_i \mathrm{EM}_i} \qquad i = 1, \ \ldots.., \ N_{bin} \tag{1}$$

where T_i and EM_i are, respectively, the central temperature and the emission measure value in the ith bin of the EM(T) distribution, N_{bin} is the number of bins, and $\sum_i \mathrm{EM}_i = \mathrm{EM}_{sum}$ is the total emission measure. The average temperature $< T >$ is typically very close to the temperature of maximum emission measure, being the EM(T) characterized by the same general trend with one maximum.

Figure 3 shows the evolution of $< T >$ and EM_{sum} during the solar cycle for the WSC (panel a) and for the BKC, ARs, and COs (panels b, c, d, respectively), in our data set. From maximum to minimum of the solar cycle the average temperature of the emitting plasma $< T >$ in WSC decreases from $\sim 2 \times 10^6$ K to slightly less than $\sim 10^6$ K and the corresponding integrated emission measure EM_{sum} decreases by a factor ~ 40.

The EM(T) evolution of the WSC is obviously due to the evolution of the regions which compose the corona. One is interested to understand if the evolution of the EM(T) of the WSC is common to all the three classes of structures or if they, as a class, follow different evolutions. We have, therefore, derived the EM(T) for all the classes of structures and for all the data of our sample.

Figure 4 shows, as examples, the EM(T) distributions derived for the WSC and the composing regions on 13 January 1992 (during the maximum of the solar cycle) and on 19 December 1995 (during the minimum). The upper panels in the figure show that different coronal regions can have very different EM(T): the COs (absent during the minimum of the solar cycle, see lower panels) are characterized by a sharp peak in the distribution at $T \gtrsim 2 \times 10^6$ K, whereas the BKC (present in both the cases considered) have an EM(T) peaking at $T \sim 1.5 \times 10^6$ K; the EM(T) of the ARs peaks at a temperature between that of the BKC and of COs. During the maximum of the solar activity, the dominant contribution to the EM(T) of the WSC appears to come from the ARs (upper panels in Fig. 4), and during the minimum from the BKC (lower panels).

Figure 3 shows that the EM(T) distributions of the BKC change the least, their $< T >$ varying within a factor 2 around 10^6 K during the cycle and their EM_{sum} within one order of magnitude around $\mathrm{EM}_{sum} \sim 10^{49}$ cm^{-3}. Instead $< T >$ of the ARs ranges between 1.5×10^6 K and 2.5×10^6 K during the solar cycle, and EM_{sum} decreases from $\sim 10^{50}$ cm^{-3} to $\sim 10^{47}$ cm^{-3} from maximum to minimum of the cycle. A similar trend characterizes the EM(T) of the COs but with larger fluctuations of $< T >$ (1.2×10^6 K – 5.2×10^6 K) and systematically lower values of EM_{sum} ($\sim 3 \times 10^{49}$ cm^{-3} – 10^{47} cm^{-3}).

As shown in Fig. 3, the ARs are the larger contributors to the EM(T) of the WSC during the maximum of the solar cycle, and mostly determine the $< T >$ of the WSC. The BKC and the COs have a similar weight in contributing to the EM(T) of the WSC during the maximum but at different temperatures. During the minimum of activity, the BKC is the only region contributing to the EM(T) of the WSC, the emission measure of the other regions being negligible.

In the light of the above results, the EM(T) of WSC at $T \gtrsim 2 \times 10^6$ K decreases rapidly (three orders of magnitude), as the cycle progresses toward the minimum, because of the gradual disappearance of ARs and of COs from the solar corona while the BKC contribution around $T \sim 1.5 \times 10^6$ K is roughly constant. This combined evolution of the various classes also leads to a steepening of the descending part of EM(T) of the WSC during the minimum.

5. X–ray Spectra and Luminosity

The EM(T) of the WSC and of the three classes of regions, and the MEKAL spectral code have been used to synthesize the X–ray spectrum of the Sun. Fig. 5 shows, as an example, the parent spectra (top panels) and the same spectra folded through the instrumental response of ROSAT/PSPC and ASCA/SIS for the Yohkoh/SXT observations on 13 January 1992, shown in Fig. 4. The spectra are synthesized in the $0.1 - 10$ keV band. We assumed in these and the following simulations that the Sun is at a distance of 1 pc. The total flux of the WSC is ~ 0.058 photons s^{-1} cm^{-2}, of the BKC ~ 0.013 photons s^{-1} cm^{-2}, of the ARs ~ 0.041 photons s^{-1} cm^{-2}, and of the COs ~ 0.003 photons s^{-1} cm^{-2}. Each panel in the figure compares the contribution of each class (thick line) to the WSC spectrum (thin line). Since the Sun is close to the maximum of the cycle, as already mentioned, the dominant contribution to the total spectrum comes from the ARs.

We adjusted the exposure times in order to have a total count of photons of ~ 4000 for ROSAT/PSPC and ~ 5000 for ASCA/SIS, typical of a good observation, and adequate to a spectral analysis with the instruments selected.

5.1. ROSAT/PSPC

In Fig. 6 we show L_{PSPC}, namely the X–ray luminosity in the ROSAT/PSPC spectral band ($0.1 - 3$ keV), of the WSC and of the three classes of regions selected (the figure also shows the X–ray luminosity in the ASCA/SIS spectral band, discussed later); for WSC, the L_{PSPC} ranges between 5×10^{27} erg s^{-1} and 10^{26} erg s^{-1}, decreasing from the maximum to the minimum of the solar cycle and reflecting the general trend of the SXT light curve in Fig. 1. This variation is mainly due to the changes of ARs and COs in the solar corona: the L_{PSPC} of the BKC decreases by just a factor 3 from the maximum to the minimum of the solar cycle, whereas the L_{PSPC} of the ARs and COs decreases by almost 3 orders of magnitude.

Fig. 5 shows the simulated ROSAT/PSPC spectra of the various classes of regions of 13 January 1992 (Fig. 4). In each panel, we compare the contribution of each region to the WSC spectrum. Although their global contribution is not large, the major contribution of the BKC and of the COs to the total spectrum is at energies below 0.3 keV and above 0.5 keV, respectively.

The dominant contribution to the EM(T), X–ray luminosity and spectra of the WSC comes from the ARs during the maximum of the cycle (before 1995) and from the BKC during the minimum. Note that the contribution of the COs is never dominant during the entire cycle for the Sun.

5.1.1. Multi–Components Spectral Fitting

The simulated ROSAT/PSPC focal plane spectra have been fitted with multiple isothermal MEKAL spectra (typically 1– or 2–temperature models), a standard method of stellar physics, excluding the channels with low signal[4] (less than 3 photons) for an appropriate evaluation of χ^2 (see Paper II). We used the spectral fitting package XSPEC V10.0 (Arnaud 1996) for our analysis. We have excluded the spectra synthesized from EM(T) distributions derived from less than 100 Yohkoh/SXT pixels (as it happens for COs close to the minimum of the cycle) because subject to large statistical uncertainties. The results are in Table 1 and in Figs. 7 and 8 together with the analogous results obtained for the ASCA/SIS synthesized spectra, discussed later.

All the synthesized spectra are well fitted with one or two different isothermal components, as it is the case, typically, with late–type stars spectra (Schmitt et al. 1990). Note that the success of this simple model fitting, in spite of the fact that the underlying EM(T) distributions are at high temperature resolution (and most likely continuous for real stars), is determined by the limited spectral capabilities of the instrument[5]. In this context, the parameters of the best–fit model (i.e. temperatures and emission measures of the isothermal components) reflect the average properties of the underlying EM(T) distribution (e.g. its maxima, see Paper II).

Our analysis shows that, as for the WSC, the two components have temperatures, T_{low} and T_{high}, in the $0.5-2\times10^6$ K and $1-5\times10^6$ K ranges, respectively, and emission measures in the $0.5-10\times10^{49}$ cm^{-3} range, with the emission measure of the hot component, EM$_{high}$, slightly lower than that of the cold component, EM$_{low}$. In the cases of low activity corona, characterized

[4]We also excluded the first two channels of ROSAT/PSPC from the analysis because they are typically affected by systematic errors.

[5]This statement is generally true for all the instruments with low spectral resolution like ROSAT/PSPC or ASCA/SIS.

by a narrower EM(T) distribution (like the one shown in the lower panels in Fig. 4) just one component, with T in the range $0.5 - 2 \times 10^6$ K, is sufficient to fit the spectra, in analogy with the coronae of less active late–type stars observed with ROSAT/PSPC (Micela, Pye & Sciortino 1997).

In the case of the BKC, both the isothermal components have $T < 2 \times 10^6$ K, and in many cases one component is sufficient to achieve a good spectral fitting. The ARs are characterized by a cold component with $T < 2 \times 10^6$ K and by a hot component with T ranging between 10^6 K and $\sim 5 \times 10^6$ K. In the case of the COs, the cold component mostly often occurs between 1 and 2×10^6 K and the hot component above 3×10^6 K. Note that, as shown in Fig. 8, the COs yield the lowest values of emission measure and, at variance with the other two kinds of structures, their EM_{high} is not systematically lower than EM_{low}.

Since we know the EM(T)'s from which we synthesize the X–ray spectra, we can check how much of these distributions is recovered with the analysis of ROSAT/PSPC data. To this end, we define the emission measure weighted temperature, $< T >_{fit}$, and the total emission measure, EM_{fit}, of the fitting components as

$$< T >_{fit} = \frac{\mathrm{EM}_{low} T_{low} + \mathrm{EM}_{high} T_{high}}{\mathrm{EM}_{low} + \mathrm{EM}_{high}} \tag{2}$$

$$\mathrm{EM}_{fit} = \mathrm{EM}_{low} + \mathrm{EM}_{high} \; . \tag{3}$$

For each of the spectra analyzed, we compare the values of $< T >_{fit}$ and EM_{fit} with the values of $< T >$ and EM_{sum} derived from the EM(T) (see Eq. 1). The good correspondence found in all the cases (differences within 17% for both $< T >_{fit}$ and EM_{fit}) shows that ROSAT/PSPC detects almost the whole contribution of the EM(T) to the X–ray emission.

5.1.2. X–ray Surface Brightness and Spectral Hardness

Schmitt (1997) and Micela et al. (1997) have studied the total X–ray surface flux in the ROSAT/PSPC band vs. the observed ROSAT/PSPC spectral hardness defined as

$$\mathrm{HR} = \frac{H - S}{H + S} \tag{4}$$

where S are the total counts in the band $0.13 - 0.40$ keV (PSPC pulse height channels 11-41) and H are the total counts in the band $0.55 - 1.95$ keV (channels 52-201). Schmitt (1997) and Micela et al. (1997) have shown a correlation of F_{PSPC} vs. HR. In Paper II we have derived a similar correlation for the few cases studied there and the comparison with the results reported in Schmitt (1997) has shown that these cases fall well in the scenario of less active stars.

It is worth exploring whether the above correlation is still present for the larger sample of data we are analyzing in this paper. Moreover, we are interested in determining the ranges of hardness ratio and of X–ray surface flux populated by the classes of regions in the solar corona. We define the X–ray surface flux in the ROSAT/PSPC band, F_{PSPC}, dividing L_{PSPC} derived from the fitted isothermal components by the area occupied in the images of the corresponding selected region[6]. Note that considering the X–ray surface flux of a given class of regions is virtually equivalent to assume that the star is completely covered by this class of regions.

In the upper panel in Fig. 9 we plot F_{PSPC} vs. HR for the WSC (crosses), the BKC (triangles), the ARs (squares), and the COs (circles). For comparison, we also plot the area of the diagram (dashed line) covered by the F, G, K, and M stars within 13 pc from the Sun (Schmitt 1997). As anticipated in Paper II, for the WSC there is a correlation between F_{PSPC} and HR which fit well in the stellar scenario, implying that the Sun is a very typical low activity late–type star; the Sun during the cycle populates the hardness ratio range between $-1 < \mathrm{HR} < -0.7$ and X–ray surface flux is correlated with HR, ranging between 10^3 and 10^5 erg cm^{-2} s^{-1}.

On the other hand, the classes of regions selected in the solar corona do not show a trend similar to that of the WSC: the BKC covers a very narrow range of HR between -1 and -0.9 with F_{PSPC} ranging between 10^4 and 10^5 erg cm^{-2} s^{-1}. The narrow range of HR simply reflects the fact that, as discussed in Sect. 4, the BKC is strongly characterized, in practice, by a single value of $< T >$. The X–ray surface flux is practically constant during the solar cycle or, in other words, BKC close to the minimum of the solar cycle are as intense as they are close to the maximum. The X–ray luminosity, L_{PSPC}, of a star identical to the Sun and totally covered by BKC would range between 1.0 and 3.8×10^{27} erg s^{-1}.

The ARs are clustered in the ranges $-1 < \mathrm{HR} < -0.7$ (analogously to the WSC) and 6×10^4 erg cm^{-2} s^{-1} $\lesssim F_{PSPC} \lesssim 1.6 \times 10^5$ erg cm^{-2} s^{-1}. For ARs, there is no strong correlation between HR and F_{PSPC} and there is no evident trend along the solar cycle. Analogously to the BKC, the ARs intensity does not change much during the solar cycle. The X–ray luminosity, L_{PSPC}, estimated for a "Sun twin" totally covered by ARs ranges between 3.8 and 9.6×10^{27} erg s^{-1}.

The COs populate the high–HR intermediate–F_{PSPC} part of the stellar distribution of Fig. 9, with a large spread of HR values ($-1 \lesssim \mathrm{HR} \lesssim 0$) and an X–ray flux ranging between 8×10^5 erg s^{-1} cm^{-2} $\lesssim F_{PSPC} \lesssim 4 \times 10^6$ erg s^{-1} cm^{-2}. The large spread in HR of COs cannot be simply explained with the fact that the relevant EM(T) distributions are subject to larger fluctuations than those of the other regions but rather with the evident correlation between HR and F_{PSPC}: decreasing F_{PSPC} is correlated with increasing HR. Such a correlation does not depend on the solar cycle, but it rather seems related to the evolution of the COs (Orlando et al. 2000b). In particular, the core of an active region has a very high HR during its emergence, implying a high average temperature $< T >$, and as the active region evolves its $< T >$ decreases. During the

[6]In the case of the WSC, the surface area is that of the Sun.

maximum of the solar activity, several active regions are present simultaneously in the corona, each of them in a different phase of its evolution: the global EM(T) reflects the weighted average of various COs at different phases of evolution. On the other hand, during the minimum of the solar cycle, there are very few ARs in the corona. If only one is present the relevant EM(T) of the core just reflects the distribution at a given phase of a single core evolution.

For the sake of completeness, we have also simulated the ROSAT/PSPC spectra taking into account the Interstellar Medium (ISM) absorption column density, N_H (as in XSPEC V10.0; see also Morrison and McCammon 1983). We considered two representative cases for N_H: 10^{18} and 10^{20} atoms/cm^2. The simulated focal plane spectra have been fitted with multiple isothermal MEKAL spectra, taking also into account N_H. We have found that an ISM absorption column density of 10^{18} atoms/cm^2 has negligible effects on the ROSAT/PSPC spectra above 0.1 keV and there are no significant changes in the F_{PSPC} vs. HR diagram: the relevant results are virtually coincident with those for $N_H = 0$ atoms/cm^2 shown in Fig. 9. On the other hand, for $N_H = 10^{20}$ atoms/cm^2, the ISM absorption has significant effects up to 1 keV. The lower panel in Fig. 9 shows the F_{PSPC} vs. HR diagram derived in this case. The effect of the ISM absorption is evident comparing this diagram with the analogous one for no ISM absorption (upper panel in the figure): the data points are systematically shifted towards higher HR values, because the ISM absorption reduces the X–ray flux in the lower energy ROSAT/PSPC channels.

5.2. ASCA/SIS

Analogously to what done for ROSAT/PSPC, Fig. 6 shows the solar X–ray luminosity in the ASCA/SIS band[7] ($0.5 - 10$ keV), L_{SIS}, during the solar cycle.

The comparison shows that L_{SIS} of the WSC is systematically lower than L_{PSPC} (cf. Fig. 6) and it decreases more than two orders of magnitude from the cycle maximum ($L_{SIS} \sim 10^{27}$ erg s^{-1}) to the minimum ($L_{SIS} \sim 10^{25}$ erg s^{-1}), implying that the Sun at minimum appears one order of magnitude fainter in the ASCA/SIS band than in the ROSAT/PSPC band. These differences can be understood in the light of the different sensitivities, spectral resolution and spectral bands of the two observatoires. In particular, ROSAT/PSPC is sensitive to photons between 0.1 and 2 keV, whereas ASCA/SIS in the band $0.5 - 10$ keV (cf. Fig. 5). The latter is less sensitive to lower temperature plasma which dominates the coronal emission at the minimum. This effect is clear from the BKC light curve. ASCA/SIS would detect the cool BKC emission as rather weak, while the hotter ARs and COs are brighter. Fig. 5 also shows the ASCA/SIS spectra derived from the EM(T) distributions of 13 January 1992 (see Fig. 4).

[7]The first 18 channels of ASCA/SIS below 0.5 keV are discarded because they are affected by systematic errors.

5.2.1. Multi–Components Spectral Fitting

We have used XSPEC V10.0 for the spectral fitting of the ASCA/SIS spectra with multiple isothermal MEKAL spectra, excluding from the analysis the spectra synthesized from EM(T) distributions derived from less than 100 Yohkoh/SXT pixels (as done for ROSAT/PSPC). The energy channels are grouped together (using the FTOOLS V4.0 manipulation tasks) so as to have at least 20 photon counts per channel, and the empty ones or those flagged as "bad" by the first data reduction are discarded. The results of the spectral fittings for the complete dataset are in Table 1 and in Figs. 7 and 8.

Most of the ASCA/SIS spectra of the WSC and of the classes of regions selected can be well fitted with two isothermal components[8]. In general, the fitting components have T higher and EM lower than those found with ROSAT/PSPC. This characteristic is particularly evident in the case of the BKC: Figs. 7 and 8 show that the temperature (emission measure) of both the cold and the hot components are systematically higher (lower) than those found with ROSAT/PSPC. In the case of ARs and COs, this difference reduces with increasing temperature of the regions, and the effect is lower in the case of COs. The explanation again is that the ASCA/SIS band, being harder than the ROSAT/PSPC one, is less sensitive to lower temperature plasma.

6. Discussion and Conclusions

In the context of the solar–stellar connection in the X–ray band, we have investigated the contribution of different classes of coronal regions resolved on the Sun to the EM(T) of the whole corona (WSC) and to the X–ray spectrum of a star identical to our Sun.

To this end, we have analyzed a sample of solar data collected with Yohkoh/SXT during the period ranging from the maximum (December 1991) to the minimum (April 1996) of solar cycle 22, in order to cover virtually the whole range of solar activity. We have selected different classes of coronal regions, namely background corona (BKC), active regions (ARs), and cores of active regions (COs), according to a criterion based on the SXT pixel intensity. Our criterion is similar to that adopted by Hara (1996) and Drake et al. (2000) and it differs only for the intensity threshold values chosen to identify the different classes of regions. For all the data of our sample, we have derived the EM(T) distributions of the WSC and of the three kinds of regions; then, we have synthesized the corresponding parent spectra and the focal–plane spectra that ROSAT/PSPC and ASCA/SIS would collect, with a realistic assumption on the count statistics appropriate for a good stellar observation.

The EM(T) of WSC is subject to large variations during the solar cycle: the relevant emission

---

[8]The only exception is the solar corona observed the 19 December 1995, during the minimum: the spectra of the BKC and of the few faint ARs present in the corona can be fitted with a single component.

measure weighted temperature $< T >$ and the total EM_{sum} decrease with the coronal activity by factors 2 and 40, respectively. The amount of plasma above 10^6 K decreases drastically as the cycle progresses to the minimum, the decrease being swifter and swifter for hotter and hotter plasma: the EM(T) distribution steepens.

This evolution of the EM(T) can be explained by the varying relative weights of the coronal regions present on the Sun along the cycle. The $< T >$ of the classes of regions selected increases from the BKC ($\sim 10^6$ K), to the ARs ($\sim 2 \times 10^6$ K), to the COs ($\sim 2 - 4 \times 10^6$ K). The BKC contribution to the EM(T) distribution of the WSC does not change appreciably whereas the contribution from ARs and COs decreases by several orders of magnitude with the solar cycle. While ARs cover only a minor fraction of the solar surface (~ 30 % during the maximum and ~ 0.1 % during the minimum), they dominate the EM(T) in the temperature range $2 - 5 \times 10^6$ K and are the main cause for the variation of the EM(T) of the WSC with the solar cycle.

The above characteristics have their effects also on the parent spectra derived from the EM(T). The focal–plane spectra are generally well fitted with 2–T models of optically thin plasma. The best–fit temperatures derived from the ASCA/SIS spectra are systematically higher than those derived from the ROSAT/PSPC spectra mostly because of the different spectral band of the two instruments, an effect very evident in the case of the BKC.

Our approach allows us to compare the best–fit values of T and EM with the original EM(T) distributions so to have a feedback on the fitting results and their implications. In Paper II we found that these values may correspond to the maxima of EM(T), if two maxima are present, or they both cluster near the maximum of EM(T). The EM(T)'s in this paper have a single maximum and we find that the average temperature $< T >$ is very close to the temperature of the maximum and is invariably between T_{low} and T_{high}; furthermore the difference $T_{high} - T_{low}$ depends on the width of the distribution and may, therefore, be interpreted as a proxy of the width when T_{high} is close to T_{low}.

In all the cases examined (even for the hottest region selected, the COs) the hot component is significantly colder than that of more active stars ($T > 10^7$ K; see, for example, Schmitt et al. 1990; Ottmann & Schmitt 1994; Kuerster & Schmitt 1996) and the emission measure of the hot component is never larger than that of the cool component, at variance with the most active stars.

Fitting ROSAT–like spectra of the Sun, along its cycle, yields results similar to those found by Micela et al. (1997) for 12 nearby halo and old disk dM stars observed with ROSAT/PSPC: the coronal emission of these stars is consistent with a 1–T or 2–T model and any variability (if present) is consistent with rather small changes of the two temperatures but large changes of the relevant emission measures. The X–ray surface flux F_{PSPC} of the halo stars ranges between that of the BKC and that of the ARs ($2 \times 10^4 - 10^5$ erg s^{-1} cm^{-2}; cf. Fig. 9); the F_{PSPC} of the old disk stars, instead, ranges between that of the ARs and that of the COs ($2 \times 10^5 - 2 \times 10^6$ erg s^{-1} cm^{-2}).

Analogously to what Micela et al. (1997) found for the old disk dM stars, we find that the emission measures of the two isothermal components fitting the ROSAT/PSPC spectra of the Sun are related according to the law (cf. Fig. 8):

$$\log(\mathrm{EM}_{high}) = A + B \log(\mathrm{EM}_{low}) \ . \tag{5}$$

Through a minimum χ^2 fitting of the data points, we have found $B \sim 1$ for all the classes of regions examined (i.e. the WSC, the BKC, the ARs, and the COs): the emission measure of the hot component changes proportionally to that of the cold component. Micela et al. (1997) studied the three stars of their sample whose data allowed this kind of analysis and found $B \sim 3$. The variability they study is, however, limited to a few hours, and mostly due to flares, while our study is dedicated to variations over a few years and due to the solar cycle. It appears, therefore, that flare variability also leads to a change of the hot component somehow coherent to that of the cool one, but the changes of the hot component are larger than those found here.

It is interesting to compare the plot of $\log F_{PSPC}$ vs. HR for the regions in the solar corona with the analogous plots derived from the stellar samples (Micela et al. 1997; Schmitt et al. 1995; Schmitt 1997). As mentioned in Sect. 5.1.2, the Sun across the cycle covers the low–HR low–F_{PSPC} part of this diagram, with a correlation HR–F_{PSPC} and fitting well in the scenario of low activity late–type stars (cf. Fig. 9). The points of each class of region are clustered in a different part of the diagram HR–F_{PSPC} and no single class shows a correlation HR–F_{PSPC} as that found for the WSC (note that when considering the F_{PSPC} of the coronal regions one may equivalently assume that the hypothetic star is totally covered by the regions under analysis).

The comparison with the results by Schmitt (1997) shows that both the F_{PSPC} and HR of BKC remains close to the minimum values derived for the stars, analogously to very low–activity stars typically detected only in the soft ROSAT/PSPC band (Schmitt 1997). F_{PSPC} and HR of ARs are both higher than those of BKC. Note that the old halo dM stars analyzed by Micela et al. (1997) have values of HR and F_{PSPC} intermediate between those of BKC and ARs.

On the other hand, the Sun entirely covered with ARs would not explain the high values of F_{PSPC} and HR of stars of intermediate–to–high activity (Fig. 9). Such values could be explained instead if a significant fraction of the stellar surface were covered by COs. Our findings, therefore, support the hypothesis that the X–ray emission of late–type stars up to intermediate activity ones are dominated by ARs and COs similar to those observed on the Sun and that the different levels of emission of these stars are simply due to a different surface coverage with solar–like ARs and COs. Drake et al. (2000) reached similar conclusions when comparing the EM(T) distributions of various solar coronal structures, as derived from Yohkoh/SXT data, with the corresponding ones of intermediate activity stars got with EUVE (*Extreme UltraViolet Explorer*) spectroscopic observations.

In conclusion, the above discussion suggests that one may explain the coronae of stars from low to intermediate activity by changing the relative weight of the different kinds of coronal regions. However, even covering entirely the stellar surface with COs one cannot explain the HR and F_{PSPC} values of very active stars. Drake et al. (2000) suggested that the very high surface density of COs in active stars would, in turn, lead to a high rate of interaction of the related magnetic structures which would lead to a high frequency of flares: the higher the rate of production of flares, the higher is the surface X–ray flux and the emission measure weighted temperature. This scenario seems to be supported by the results of Reale et al. (2000) which applies the method in Sect. 2 to a sample of solar flares of different intensity (see also Peres et al. 2000b).

Future investigations along this line are in order and, in particular, the comparison of the solar data with the ones from the instruments on board Chandra and XMM–Newton (*X–ray Multi–Mirror Mission*).

We acknowledge the anonymous referee for having taken care of the paper and for his suggestions. We are grateful to G. Micela and A. Maggio for the useful discussions. This work was supported in part by Agenzia Spaziale Italiana and by Ministero della Università e della Ricerca Scientifica e Tecnologica.

REFERENCES

Arnaud, K., 1996, Astronomical Data Analysis Software and Systems, eds. Jacoby G. and Barnes J., ASP Conf. Ser. 101, 14

Drake, J.J., Peres, G., Orlando, S., Laming, J.M., Maggio, A., 2000, ApJ in press

Hara, H., 1996, PhD Thesis, School of Science, The University of Tokyo

Kaastra, J. S. 1992, An X–Ray Spectral Code for Optically Thin Plasmas, Internal SRON–Leiden Report, updated version 2.0

Kuerster, M., Schmitt, J.H.M.M., 1996, A&A 311, 211

Mewe, R., Gronenschild, E. H. B. M., van den Oord, G. H. J. 1985, A&AS, 62, 197

Micela, G., Pye, J., Sciortino, S., 1997, A&A, 320, 865

Morrison, R., McCammon, D. 1983, ApJ 270, 119

Orlando, S., Peres, G., Reale, F., 2000a, ApJ 528, 524

Orlando, S., Peres, G., Reale, F., 2000b, in preparation

Ottman, R., Schmitt, J.H.M.M., 1994, A&A 283, 871

Pallavicini, R., Peres, G., Serio, S., Vaiana, G.S., Golub, L., Rosner, R., 1981, ApJ 247, 692

Peres, G., Orlando, S., Reale, F., Rosner, R., Hudson, H., 2000a, ApJ 528, 537

Peres, et al., 2000b, Nature in preparation

Reale, F., Peres, G., Orlando, S., 2000, ApJ submitted

Schmitt, J.H.M.M., Collura, A., Sciortino, S., et al. 1990, ApJ 365, 704

Schmitt, J.H.M.M., Fleming, T.A., Giampapa, M.S., 1995, ApJ 450, 392

Schmitt, J.H.M.M., 1997, A&A 318, 215

Tsuneta, S., et al. 1991, Sol. Phys., 136, 37

Watanabe, T., Hara, H., Shimizu, T., Hiei, E., Bentley, R. D., Lang, J., Phillips, K. J. H., Pike C. D., Fludra, A., Bromage, B. J. I., Mariska, J. 1995, Sol. Phys., 157, 169

This preprint was prepared with the AAS LaTeX macros v4.0.

Fig. 1.— Light curve of the total flux at earth, obtained from the full–disk SXT images through the thin aluminum filter. The crosses mark the data we have selected.

Fig. 2.— Intensity cumulative histogram obtained from all the 23 images in the band of thin aluminum filter of our sample. The dotted lines mark the threshold adopted to discriminate between the background corona, active regions, and cores of active regions. The dashed line marks the slope of the power law of the "active regions" portion of the histogram.

Fig. 3.— Evolution of the average temperature weighted by the emission measure $< T >$ (squares and left vertical axis) and of the integrated emission measure EM_{sum} (filled circles and right vertical axis) during the solar cycle for the whole solar corona (panel a), the background corona (panel b), the active regions (panel c), and the cores of active regions (panel d). The arrows in panel (d) show observations for which there are less than 100 pixels to determine the EM(T) distribution. The dashed and the dotted lines mark $T = 10^6$ K and EM $= 10^{49}$ cm^{-3}, respectively. Error bars are shown for each data point but they are, in most cases, rather small.

Fig. 4.— Two very different examples of emission measure distributions vs. temperature: the one for 13 January 1992 (upper panels), during the maximum of the solar cycle, and that for 19 December 1995 (lower panels), during the minimum. The left panels show the full–Sun X–ray images obtained with the thin aluminum filter and the right panels show the EM(T) distribution: background corona (BKC, dotted line), active regions (ARs, dashed), and cores of active regions (COs, thick solid). The thin solid line marks the EM(T) distribution of the whole solar corona (WSC).

Fig. 5.— Spectra of the solar corona in the $0.1-3$ keV band synthesized with the MEKAL code from the original EM(T) distributions (in Fig. 4a) of the background corona, of the active regions, and of the cores of active regions. The top panels show the parent spectra, the middle and the bottom panels the focal–plane spectra of ROSAT/PSPC and ASCA/SIS respectively, assuming the Sun at a distance of 1 pc and a total count of photons ~ 4000. Each panel also shows the spectrum of the whole solar corona (marked with a thin line). For the ROSAT/PSPC and ASCA/SIS spectra, each panel shows the simulated data (crosses) together with the best–fit multi–temperatures MEKAL spectra (solid histograms) and the contribution of each bin to the total χ.

Fig. 6.— X–ray luminosity in the ROSAT/PSPC band ($0.1-3$ keV; squares) and in the ASCA/SIS band ($0.5-10$ keV; filled circles) computed from the EM(T) distributions for the whole solar corona (panel a), the background corona (panel b), the active regions (panel c), and the cores of active regions (panel d). Analogously to Fig. 3, the arrows mark the observations for which there are less than 100 pixels to determine the EM(T) distribution. Error bars are shown for each data point but they are, in most cases, rather small.

Fig. 7.— Temperature of the hot component vs. the temperature of the cold component for the solar corona and for the various classes of regions; squares, derived from ROSAT/PSPC spectra, and crosses, derived from ASCA/SIS spectra. The arrows mark the cases fitted with only one

isothermal component (the ASCA/SIS cases are marked with empty arrows).

Fig. 8.— The same as in Fig. 7 for the emission measure values.

Fig. 9.— X–ray surface flux (erg s^{-1} cm^{-2}) in the ROSAT/PSPC band vs. the hardness ratio between soft and hard PSPC counts for: the whole solar corona (crosses), background corona (triangles), active regions (squares), and cores of active regions (circles). The figure shows the result for negligible ISM absorption, $N_H = 0$ atoms/cm^2 (upper panel), and for $N_H = 10^{20}$ atoms/cm^2 (lower panel). The dashed gray curve in the upper panel marks the region of the diagram populated by the F, G, K, and M stars within 13 pc from the Sun (Schmitt 1997).

Table 1. Analysis of Stellar–like Solar Spectra

	ROSAT/PSPC							ASCA/SIS						
	t_{exp} (s)	N_{chan}	$\overline{\chi}_r^2$	T_1 (10^6 K)	T_2	EM_1 (10^{49} cm^{-3})	EM_2	t_{exp} (10^3 s)	N_{chan}	$\overline{\chi}_r^2$	T_1 (10^6 K)	T_2	EM_1 (10^{49} cm^{-3})	EM_2
16-Dec-91														
WSC[a]	490	23	0.67	1.12	2.58	9.76	7.68	16	30	1.24	2.17	6.74	8.853	0.723
BKC[b]	4641	20	0.66	0.62	1.46	1.15	0.77	726	26	1.14	1.66	4.64	0.374	0.021
ARs[c]	671	23	0.79	1.47	3.77	9.35	1.31	24	29	0.89	2.11	6.26	6.770	0.460
COs[d]	3162	24	0.81	1.96	5.49	2.34	0.55	54	32	1.48	2.31	5.66	2.094	0.305
06-Jan-92														
WSC	411	26	0.58	1.14	2.80	12.7	7.55	14	30	0.88	2.11	5.32	9.924	1.295
BKC	6172	22	0.73	0.63	1.40	0.77	0.61	970	28	1.31	1.68	5.64	0.288	0.013
ARs	790	22	0.55	0.90	2.23	3.69	6.97	24	29	0.79	2.04	4.52	6.556	0.843
COs	4008	25	0.83	1.59	3.28	0.63	1.87	46	33	0.58	2.51	5.87	1.634	0.473
13-Jan-92														
WSC	609	23	0.97	1.01	2.56	7.78	6.07	21	28	0.67	2.02	4.01	6.558	1.282
BKC	3772	22	0.56	0.67	1.42	1.61	0.70	726	28	1.41	1.64	5.64	0.434	0.015
ARs	814	25	0.52	1.45	2.62	6.91	3.15	27	27	0.58	1.80	3.30	6.203	1.550
COs	7610	25	0.77	1.97	3.14	0.56	0.70	104	30	0.87	2.51	4.33	0.823	0.231
27-Feb-92														
WSC	661	25	0.83	1.64	4.60	9.33	2.31	18	30	0.61	2.26	6.70	7.403	0.628
BKC	7204	20	0.75	0.93	2.22	0.89	0.20	794	27	1.17	1.71	5.74	0.351	0.017
ARs	890	24	0.58	1.48	2.87	5.74	3.50	23	28	0.93	2.13	4.28	6.294	0.780
COs	4159	24	0.48	0.95	3.07	1.14	1.03	90	31	1.75	2.41	5.37	0.861	0.282
03-May-92														
WSC	1431	24	0.52	1.22	2.31	3.29	2.40	55	29	0.61	2.08	6.13	2.976	0.210
BKC	6225	17	0.99	0.92	1.76	0.87	0.36	751	26	1.43	1.72	6.18	0.381	0.008
ARs	2141	21	1.04	1.71	4.27	3.34	0.35	73	30	0.70	2.08	5.33	2.217	0.191
COs	14779	29	0.26	1.81	7.18	0.49	0.07	352	33	0.99	2.19	6.15	0.331	0.056
12-Aug-92														
WSC	1473	21	0.66	1.16	2.37	3.39	1.91	63	28	0.76	1.83	4.34	2.880	0.405
BKC	4979	19	1.03	0.55	1.34	0.67	1.07	681	27	1.35	1.70	6.68	0.439	0.011
ARs	2395	22	0.89	1.21	2.40	1.74	1.57	87	29	1.58	2.10	4.40	1.767	0.186
COs	16782	25	0.68	1.45	3.83	0.33	0.18	341	37	1.23	2.09	6.92	0.259	0.079
29-Nov-92														
WSC	1297	21	0.95	1.81	-	6.03	-	47	27	0.91	1.59	3.20	4.627	1.145
BKC	5368	18	0.86	0.89	1.91	1.09	0.39	562	24	0.88	1.34	2.90	1.116	0.045
ARs	1948	26	0.62	0.97	2.19	1.58	2.67	66	27	0.96	2.02	5.22	2.608	0.230
COs	13377	24	0.91	1.99	5.88	0.55	0.11	238	29	0.79	2.21	4.43	0.449	0.114
04-Jun-93														
WSC	2132	24	0.53	1.49	3.03	2.51	1.29	63	30	0.78	2.18	5.43	2.187	0.234
BKC	8899	24	0.64	0.83	1.88	0.60	0.32	826	27	1.34	1.72	6.02	0.320	0.013
ARs	3294	25	0.97	1.56	2.68	1.54	0.98	93	29	0.84	2.15	7.05	1.659	0.116
COs	20782	25	1.07	1.56	3.57	0.17	0.30	259	34	0.62	2.46	5.63	0.308	0.093
27-Jun-93														

Table 1—Continued

	ROSAT/PSPC							ASCA/SIS						
	$t_{\rm exp}$ (s)	$N_{\rm chan}$	$\overline{\chi}^2_r$	T_1 (10^6 K)	T_2	EM_1 (10^{49} cm^{-3})	EM_2	$t_{\rm exp}$ (10^3 s)	$N_{\rm chan}$	$\overline{\chi}^2_r$	T_1 (10^6 K)	T_2	EM_1 (10^{49} cm^{-3})	EM_2
WSC	2544	26	0.97	1.76	3.66	2.57	0.61	60	30	1.01	2.09	4.91	2.307	0.344
BKC	12634	27	0.93	1.59	-	0.58	-	723	28	0.68	1.74	5.28	0.366	0.021
ARs	3833	29	0.74	2.17	-	2.29	-	89	28	0.91	1.43	3.01	2.044	0.838
COs	20834	25	1.02	1.52	3.62	0.16	0.31	254	33	0.65	2.36	5.42	0.312	0.113
27-Jul-93														
WSC	2388	20	0.86	1.23	2.31	2.12	1.10	113	27	1.44	1.75	4.37	2.119	0.172
BKC	7230	20	1.01	1.26	-	0.98	-	750	27	1.33	1.69	5.88	0.386	0.013
ARs	3797	21	0.89	1.25	2.23	1.05	1.11	144	27	0.71	2.01	5.16	1.234	0.101
COs	-	-	-	-	-	-	-	-	-	-	-	-	-	-
05-Aug-93														
WSC	1761	23	0.94	0.94	2.29	3.43	1.20	112	27	1.00	1.88	3.97	1.689	0.203
BKC	2871	15	0.74	0.55	1.21	1.89	1.42	754	19	1.06	1.31	2.59	0.920	0.029
ARs	4743	20	0.86	1.77	7.43	1.61	0.14	146	27	1.13	1.61	2.98	1.240	0.445
COs	154771	26	0.98	2.07	4.02	0.02	0.04	1390	35	0.91	2.65	6.15	0.044	0.019
01-Nov-93														
WSC	3901	21	0.64	1.08	2.25	1.19	0.82	196	26	0.93	1.86	3.30	0.914	0.179
BKC	7509	21	0.95	1.20	-	0.93	-	1010	24	0.92	1.66	5.15	0.335	0.006
ARs	8448	21	0.58	1.73	4.32	0.82	0.13	247	27	0.67	1.75	3.17	0.632	0.209
COs	-	-	-	-	-	-	-	-	-	-	-	-	-	-
24-Jan-94														
WSC	1686	21	0.67	1.20	3.09	3.43	1.47	55	31	0.80	2.17	6.60	2.661	0.232
BKC	5007	19	0.62	0.85	1.65	0.92	0.65	605	23	0.94	1.57	3.18	0.589	0.033
ARs	3395	22	0.66	1.67	3.34	1.84	0.57	88	30	1.21	2.08	5.41	1.863	0.174
COs	10729	29	0.36	1.15	3.60	0.43	0.38	198	36	1.39	2.42	6.16	0.330	0.137
18-Feb-94														
WSC	2489	20	0.52	1.04	2.35	1.83	1.48	105	27	0.92	1.38	2.82	2.345	0.755
BKC	5496	26	0.94	1.10	-	1.34	-	793	25	0.83	1.65	5.97	0.415	0.009
ARs	4832	24	1.03	2.07	-	1.73	-	127	29	0.90	1.76	3.32	1.220	0.395
COs	-	-	-	-	-	-	-	-	-	-	-	-	-	-
16-May-94														
WSC	2436	18	0.93	1.04	2.45	2.48	0.63	191	26	1.12	1.79	5.27	1.398	0.052
BKC	5537	18	0.87	0.04	1.17	2.28	1.20	891	21	1.03	1.10	2.28	1.318	0.073
ARs	4907	22	1.02	1.29	2.64	1.30	0.29	256	27	0.63	1.79	5.27	1.014	0.043
COs	-	-	-	-	-	-	-	-	-	-	-	-	-	-
01-Jun-94														
WSC	8392	17	1.03	1.20	-	0.88	-	978	21	0.98	1.41	2.33	0.499	0.044
BKC	11253	16	0.99	1.22	-	0.63	-	1482	22	0.98	1.39	2.99	0.423	0.009
ARs	35457	23	0.60	1.36	-	0.20	-	2934	22	0.85	1.09	2.22	0.410	0.028
COs	-	-	-	-	-	-	-	-	-	-	-	-	-	-
19-Sep-94														
WSC	7963	20	0.72	0.93	1.99	0.73	0.27	801	25	0.98	1.49	3.03	0.406	0.050

Table 1—Continued

	ROSAT/PSPC							ASCA/SIS						
	$t_{\rm exp}$ (s)	$N_{\rm chan}$	$\overline{\chi}_r^2$	T_1 (10^6 K)	T_2	EM$_1$ (10^{49} cm^{-3})	EM$_2$	$t_{\rm exp}$ (10^3 s)	$N_{\rm chan}$	$\overline{\chi}_r^2$	T_1 (10^6 K)	T_2	EM$_1$ (10^{49} cm^{-3})	EM$_2$
BKC	10672	16	0.46	0.82	1.77	0.64	0.16	1935	23	1.05	1.39	3.75	0.297	0.006
ARs	35791	24	0.70	0.57	1.79	0.08	0.17	1786	27	0.65	1.43	2.85	0.160	0.035
COs	-	-	-	-	-	-	-	-	-	-	-	-	-	-
12-Dec-94														
WSC	4645	24	0.79	1.15	2.96	1.19	0.55	145	34	0.82	2.13	5.73	0.728	0.173
BKC	7999	21	0.92	1.15	-	0.91	-	992	25	0.83	1.65	5.32	0.346	0.007
ARs	14546	25	0.59	1.69	3.78	0.44	0.13	359	31	0.49	2.21	5.74	0.374	0.043
COs	50122	26	0.94	3.91	-	0.23	-	323	36	0.94	3.38	5.68	0.140	0.077
02-Mar-95														
WSC	4252	24	0.96	0.95	2.47	1.35	0.56	214	29	0.72	2.06	5.75	0.730	0.069
BKC	7700	17	0.53	0.73	1.37	0.71	0.39	1605	24	0.90	1.63	6.36	0.221	0.003
ARs	9678	23	0.80	1.46	2.56	0.45	0.43	260	29	1.04	2.12	5.50	0.582	0.059
COs	-	-	-	-	-	-	-	-	-	-	-	-	-	-
31-May-95														
WSC	14836	25	0.58	1.13	2.56	0.46	0.08	1105	25	0.95	1.78	4.05	0.237	0.011
BKC	21853	22	0.53	0.94	2.02	0.30	0.08	2798	23	0.78	1.63	5.21	0.127	0.002
ARs	46436	26	0.42	1.32	2.53	0.11	0.06	1829	26	0.87	1.94	3.52	0.116	0.010
COs	-	-	-	-	-	-	-	-	-	-	-	-	-	-
02-Aug-95														
WSC	8339	25	0.41	0.93	2.21	0.70	0.30	586	27	0.83	1.96	5.43	0.333	0.020
BKC	12308	18	0.98	0.76	1.49	0.37	0.29	1912	22	0.89	1.12	2.30	0.561	0.030
ARs	26523	25	0.87	1.46	2.72	0.22	0.08	909	28	0.52	2.01	4.65	0.191	0.021
COs	-	-	-	-	-	-	-	-	-	-	-	-	-	-
19-Dec-95														
WC	9844	16	0.45	1.10	-	0.74	-	2237	20	0.51	1.31	2.87	0.322	0.006
BC	10925	14	0.70	0.99	-	0.67	-	2983	18	0.79	1.47	-	0.171	-
AR	99551	20	1.04	1.39	-	0.07	-	8953	25	0.87	1.58	2.84	0.033	0.005
CO	-	-	-	-	-	-	-	-	-	-	-	-	-	-
01-Apr-96														
WSC	7095	18	0.66	0.54	1.25	0.74	0.61	1738	20	1.19	1.32	2.77	0.414	0.010
BKC	7443	13	0.21	0.48	1.24	1.12	0.51	1999	20	0.89	1.43	3.32	0.269	0.004
ARs	194684	17	0.88	1.43	-	0.04	-	16010	22	0.96	1.66	3.41	0.023	0.000
COs	-	-	-	-	-	-	-	-	-	-	-	-	-	-

[a]Whole solar corona.

[b]Background corona.

[c]Active regions.

[d]Cores of active regions.

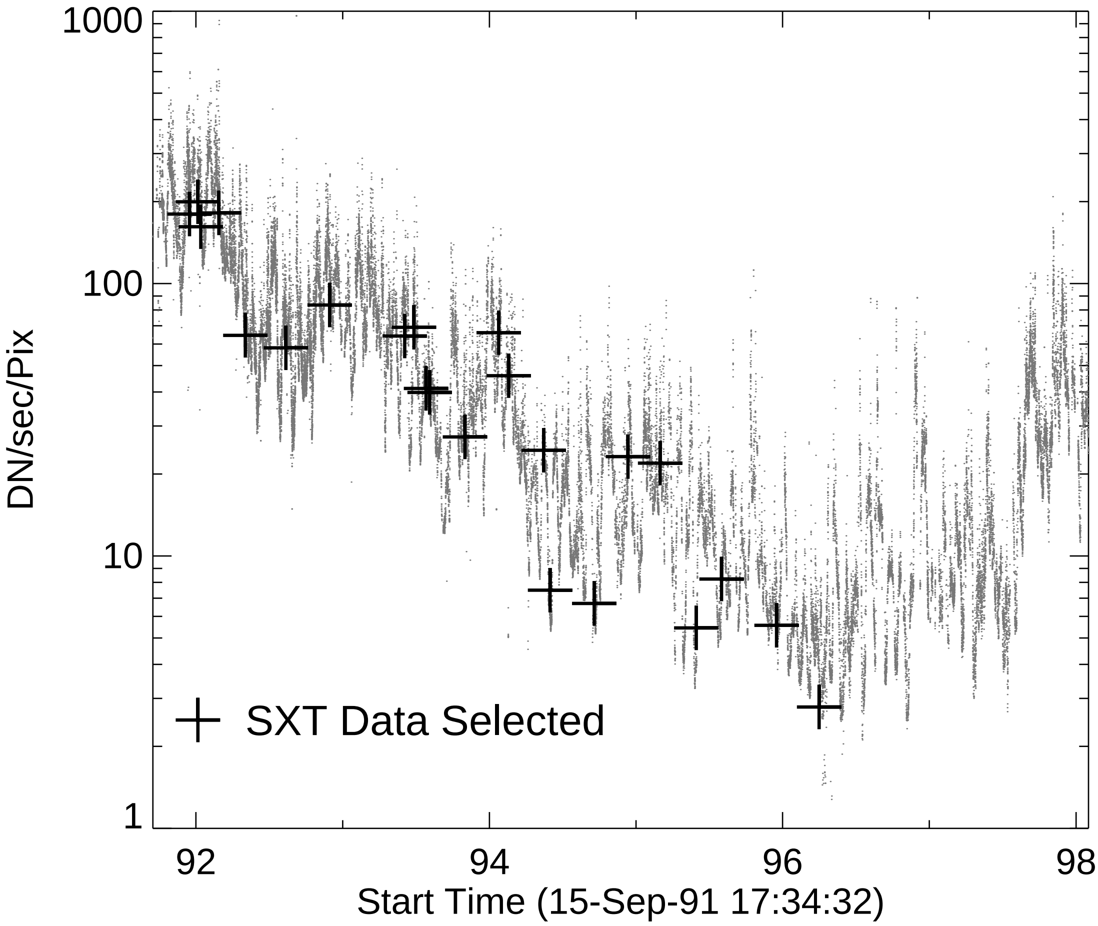
1000
100
10
1
DN/sec/Pix
92
94
96
98
Start Time (15-Sep-91 17:34:32)
SXT Data Selected

Fig. 1.—

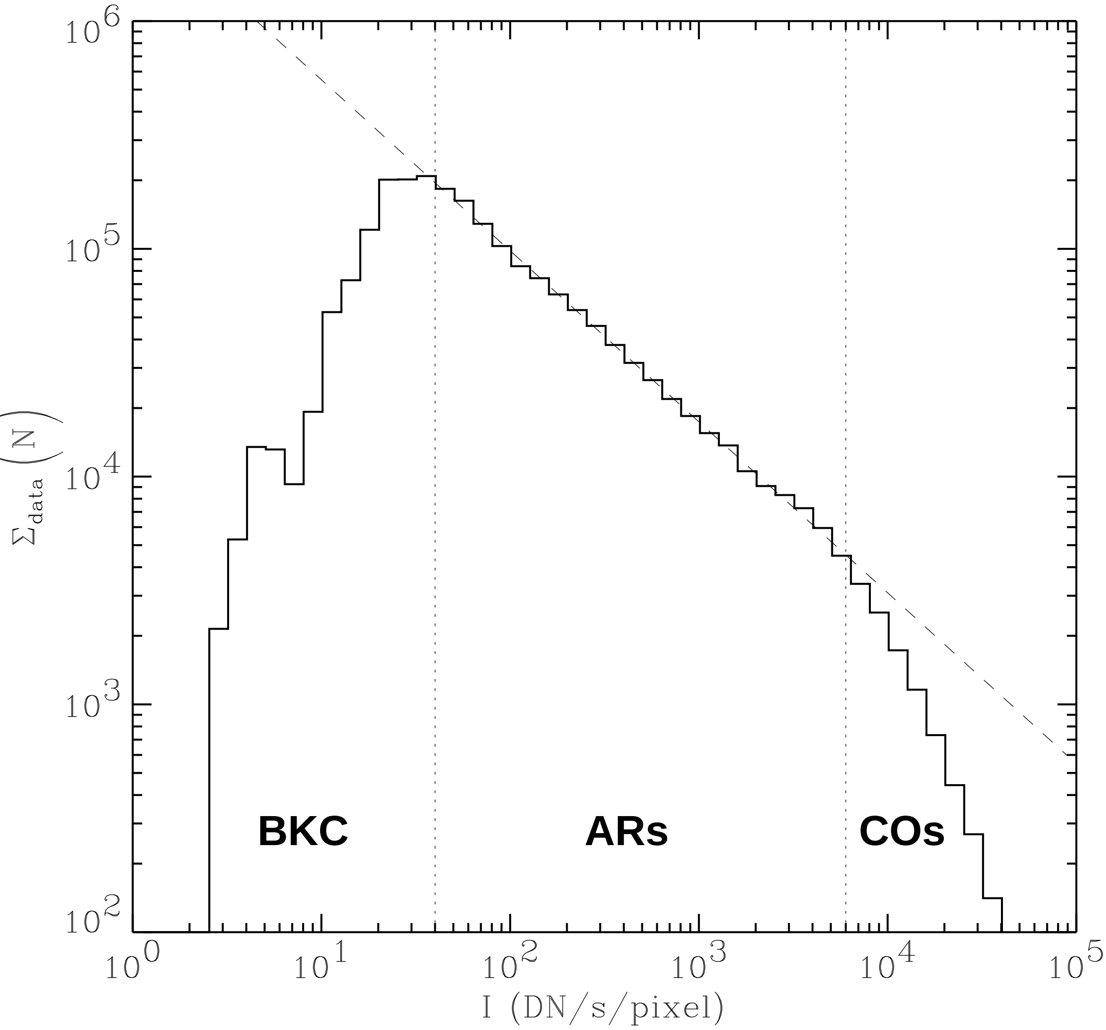

10^6
10^5
10^4
10^3
10^2
$\Sigma_{\rm data}\left(\rm N\right)$
BKC
ARs
COs
10^0
10^1
10^2
10^3
10^4
10^5
I (DN/s/pixel)

Fig. 2.—

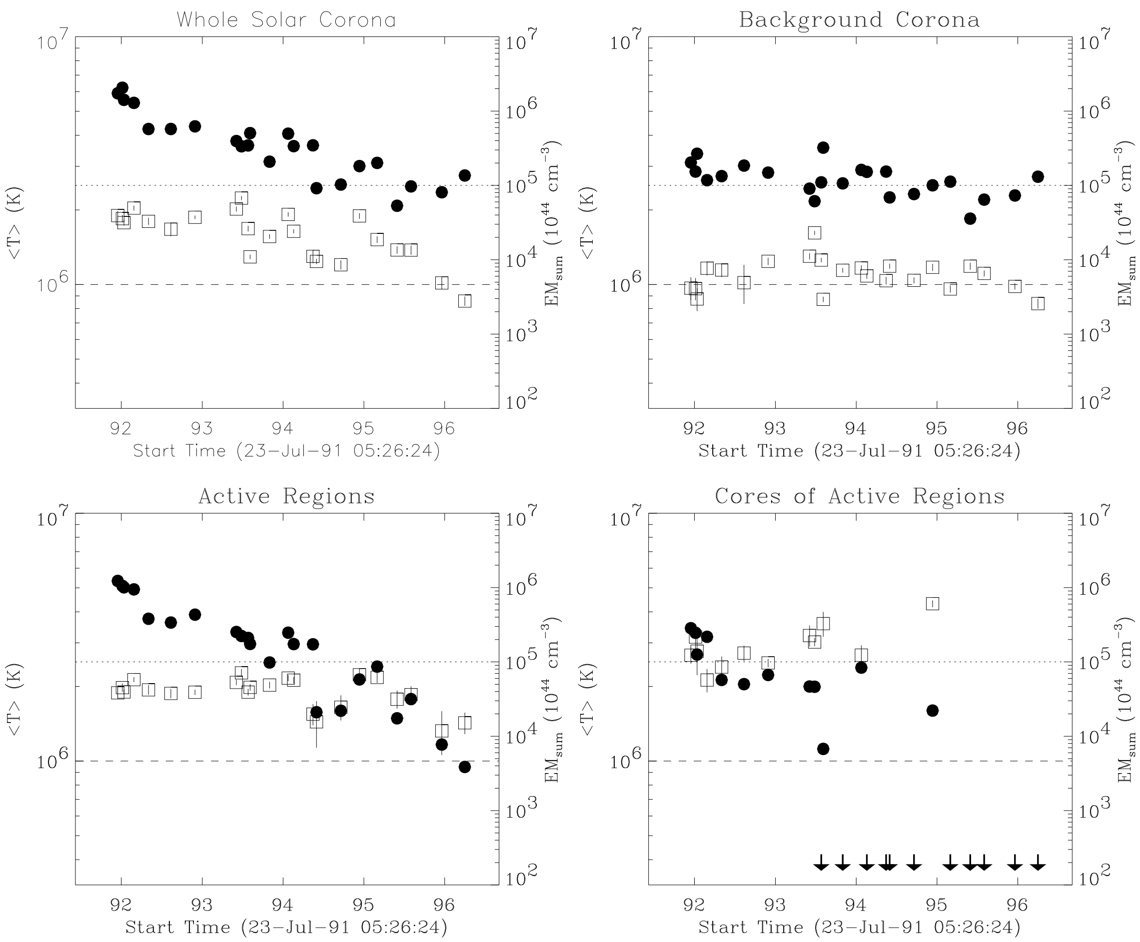
Whole Solar Corona
Background Corona
Active Regions
Cores of Active Regions
<T> (K)
EM_sum (10^44 cm^-3)
Start Time (23-Jul-91 05:26:24)
92
93
94
95
96

Fig. 3.—

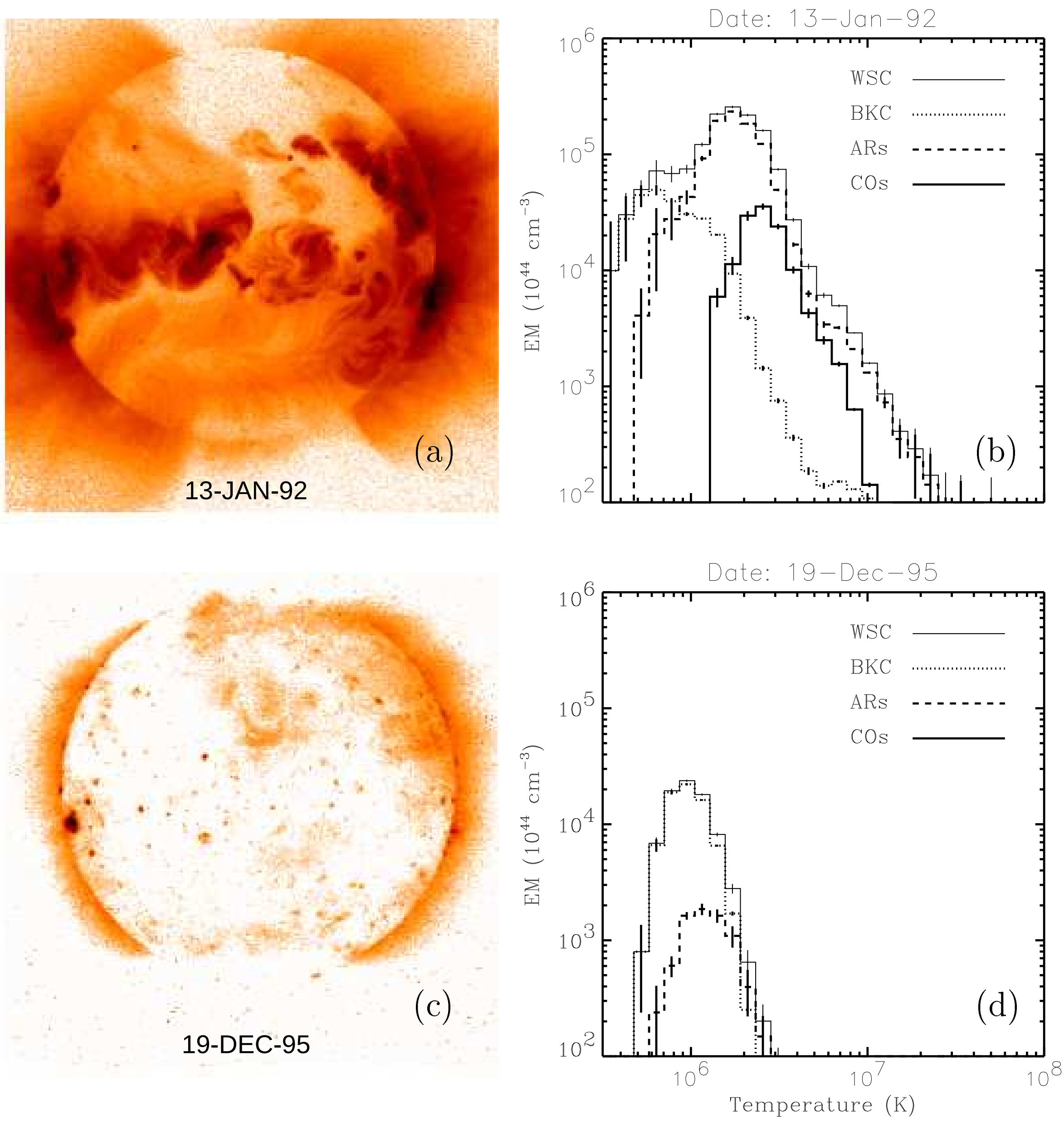
13-JAN-92
(a)
Date: 13−Jan−92
WSC
BKC
ARs
COs
EM (10^44 cm^-3)
(b)
19-DEC-95
(c)
Date: 19−Dec−95
WSC
BKC
ARs
COs
EM (10^44 cm^-3)
(d)
Temperature (K)

Fig. 4.—

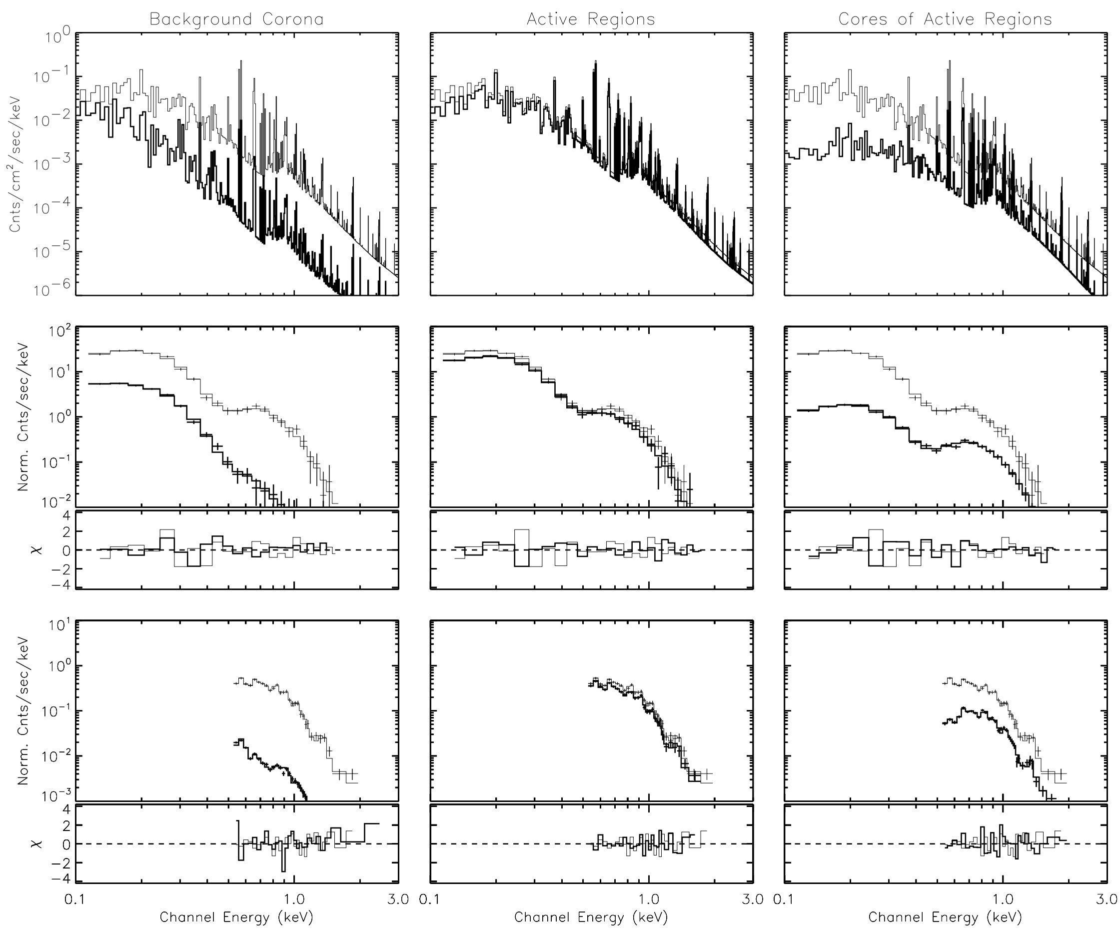

Background Corona
Active Regions
Cores of Active Regions
Cnts/cm^2/sec/keV
Norm. Cnts/sec/keV
χ
Channel Energy (keV)
0.1
1.0
3.0

Fig. 5.—

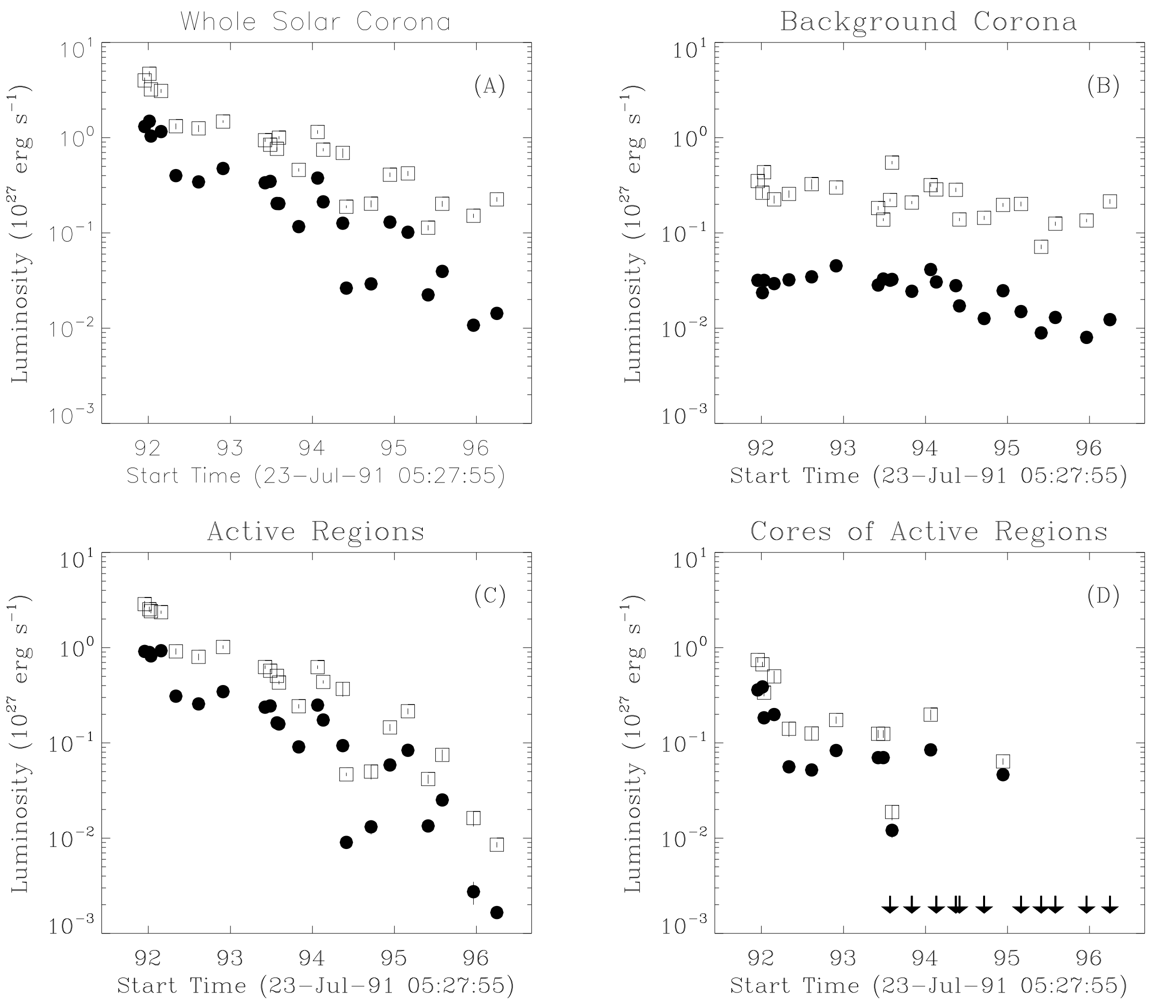
Whole Solar Corona
(A)
Luminosity (10^{27} erg s^{-1})
Start Time (23-Jul-91 05:27:55)
Background Corona
(B)
Active Regions
(C)
Cores of Active Regions
(D)

Fig. 6.—

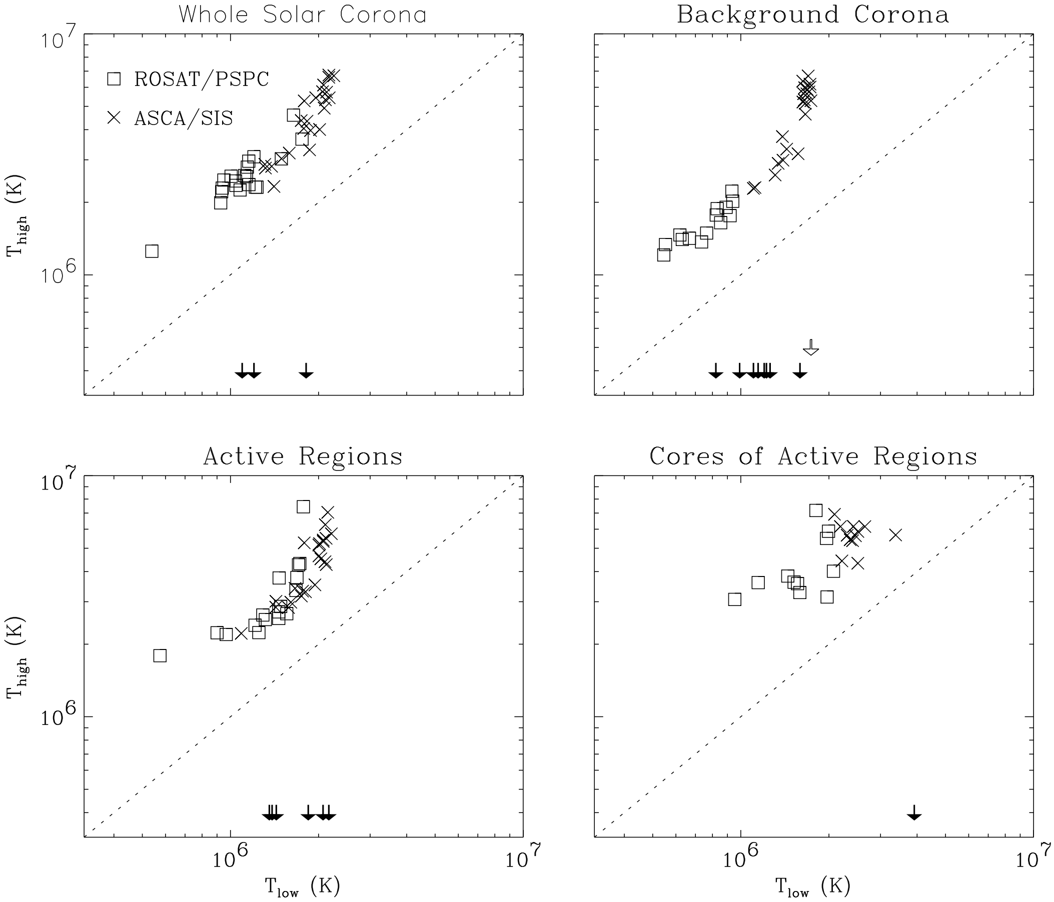
Whole Solar Corona
Background Corona
Active Regions
Cores of Active Regions
ROSAT/PSPC
ASCA/SIS
T_{high} (K)
T_{low} (K)
10^6
10^7

Fig. 7.—

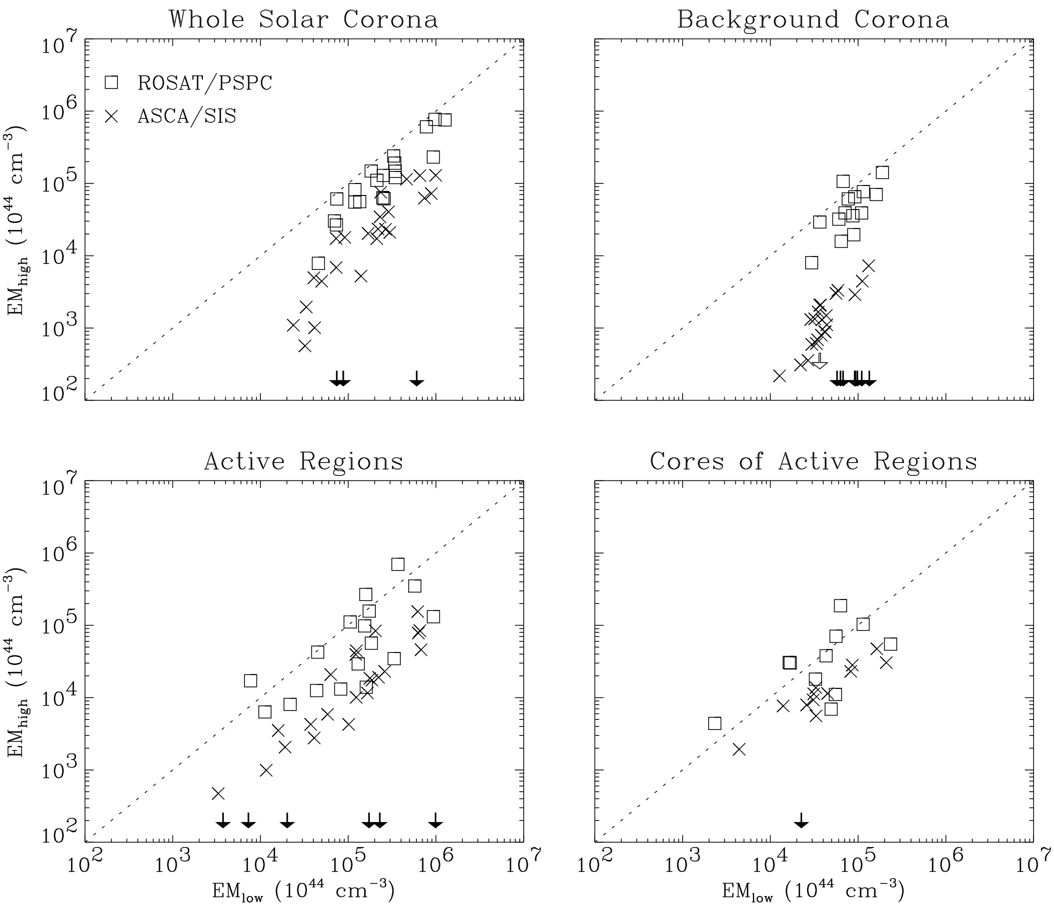

Whole Solar Corona
Background Corona
Active Regions
Cores of Active Regions
ROSAT/PSPC
ASCA/SIS
EM_{high} (10^{44} cm^{-3})
EM_{low} (10^{44} cm^{-3})
10^2
10^3
10^4
10^5
10^6
10^7

Fig. 8.—

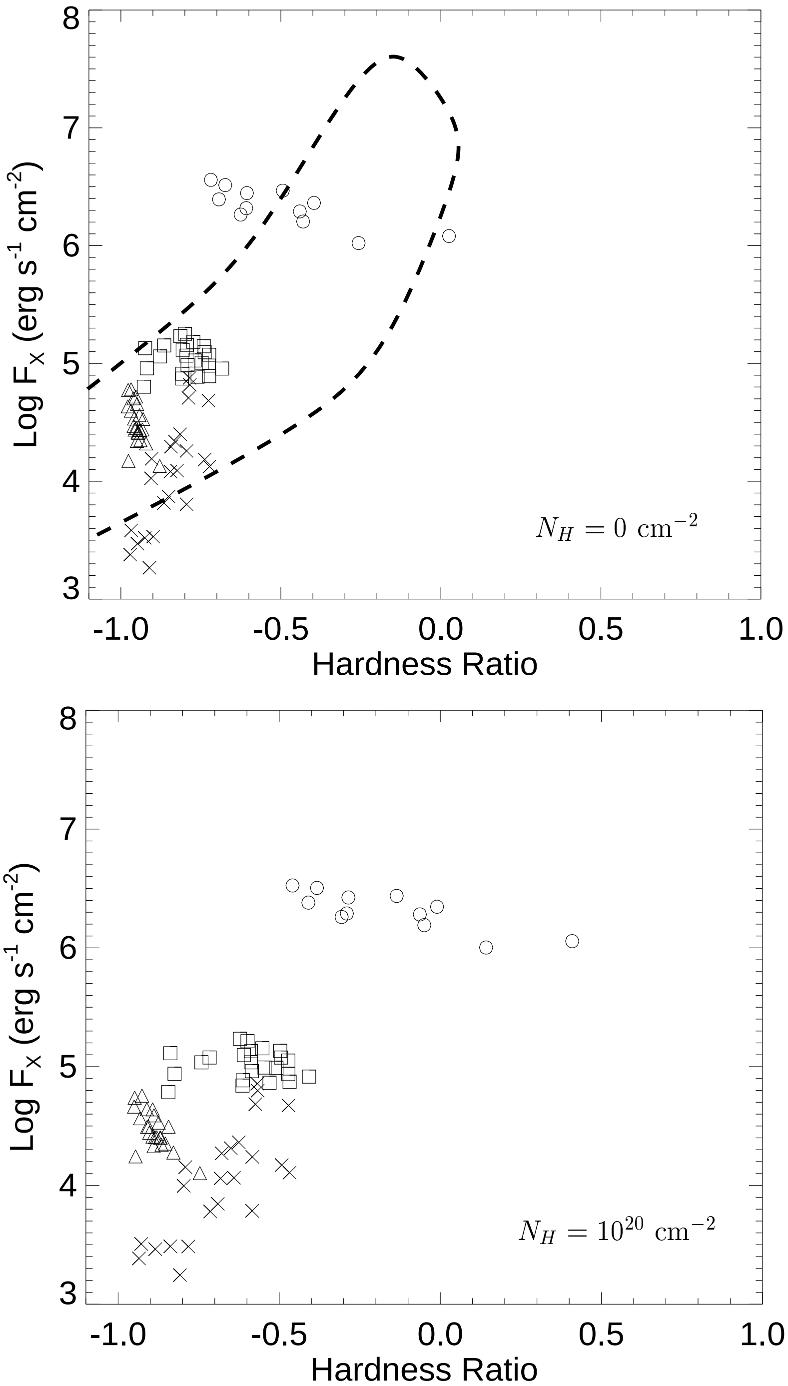
8
7
6
5
4
3
Log F_X (erg s^{-1} cm^{-2})
-1.0
-0.5
0.0
0.5
1.0
Hardness Ratio
$N_H = 0\ \mathrm{cm}^{-2}$
8
7
6
5
4
3
Log F_X (erg s^{-1} cm^{-2})
-1.0
-0.5
0.0
0.5
1.0
Hardness Ratio
$N_H = 10^{20}\ \mathrm{cm}^{-2}$

Fig. 9.—